NJC

Accepted Manuscript

This is an *Accepted Manuscript*, which has been through the Royal Society of Chemistry peer review process and has been accepted for publication.

Accepted Manuscripts are published online shortly after acceptance, before technical editing, formatting and proof reading. Using this free service, authors can make their results available to the community, in citable form, before we publish the edited article. We will replace this *Accepted Manuscript* with the edited and formatted *Advance Article* as soon as it is available.

You can find more information about *Accepted Manuscripts* in the Information for Authors.

Please note that technical editing may introduce minor changes to the text and/or graphics, which may alter content. The journal's standard Terms & Conditions and the Ethical guidelines still apply. In no event shall the Royal Society of Chemistry be held responsible for any errors or omissions in this *Accepted Manuscript* or any consequences arising from the use of any information it contains.

ROYAL SOCIETY OF CHEMISTRY

www.rsc.org/njc

One-pot synthesis of ordered mesoporous transition metals-zirconium oxophosphate composites with excellent textural and catalytic properties

Zhichao Miao[a,b], Huahua Zhao[a], Jian Yang[a], Jun Zhao[a], Huanling Song[a,c], Lingjun Chou[a,c*]

Abstract

A series of ordered mesoporous transition metals-zirconium oxophosphate composites (M-X-ZrPO, X = Cr, Mn, Fe, Co, Ni, Cu, Zn) were designed and synthesized via a facile and general one-pot evaporation-induced self-assembly (EISA) method. N_2-physisorption and TEM characterizations showed that all the final materials possessed ordered mesoporous structure accompanying with large specific surface area (170-220 $m^2 \cdot g^{-1}$), big pore volume (0.2-0.4 $cm^3 \cdot g^{-1}$) and uniform pore size (5.6-7.8 nm). Moreover, the introduced transition metals homogeneously dispersed in the mesoporous skeleton and effectively improved the mesostructure. The catalytic performance of M-X-ZrPO was evaluated in liquid phase oxidation of ethylbenzene. The introduced transition metals obviously enhanced the catalytic performance of M-ZrPO. The M-Mn-ZrPO showed excellent catalytic activity with 91.6% conversion of ethylbenzene and 87.0% selectivity of acetophenone. After five cycles, there was no notable decrease in catalytic activity. Therefore, it was a promising catalyst for oxidation of ethylbenzene.

Keywords: one-pot; ordered mesoporous materials; nanocomposites; partial oxidation.

1. Introduction

Ordered mesoporous materials (OMMs) have attracted continuous attention since the discovery of M41S family in 1992.[1,2] Owing to their superior textural properties, such as high surface areas, regular pore frameworks with large pore size and volume, OMMs have been widely developed and investigated the potential applications in fields of catalysis, separation, drug delivery and sorption.[3-6] As for synthetic methods, the "hard template" and "soft template" are common methods to obtain OMMs.[7,8] The evaporation-induced self-assembly (EISA) method, which is a typical "soft template" method and usually employed nonionic surfactants as structure-directing agents (SDAs), is extensively investigated in preparing mesoporous metal oxides and composites and the obtained mesoporous materials, such as Al-based materials, metal phosphates and TiO_2 based materials, showed outstanding catalytic performance in the CO_2 reforming of CH_4, acid-catalyzed reactions and photocatalytical applications.[9-13] This method is flexible, but expensive metal alkoxides are commonly utilized as precursors and mineral acids need to be precisely controlled as acid modifier to manage the alcoholysis process of metal precursors in the EISA process.[14] All these might limit the utilization of OMMs on a large scale.

Transition metals, which have unoccupied 3d orbits, are good electron acceptors and widely used in many fields, such as redox reactions, adsorption, solar cell and photocatalysis.[15-19] Transition metals materials with abundant ordered mesoporous pores can greatly increase the accessible active sites, which might improve their applications in these fileds. For the applications in catalytic fields, transition metals

extensively act as active sites for the oxidation reactions. The Cr-MCM-41, Mn-Ti-SBA-15, Co-SBA-16 and Cu-TUD-1 materials were synthesized and employed as catalyst in the oxidation of ethylbenzene, hydroxylation of benzene and phenol.[20-23] In consideration of the extensive applications of mesoporous transition metals materials, the facile one-pot method, which can be applied to the synthesis of ordered mesoporous composites with different kinds of transition metals, has potential to be investigated.

Herein, we employed a facile and general one-pot EISA method to synthesize ordered mesoporous transition metals-zirconium oxophosphate composites (M-X-ZrPO). Cheap and common metal chlorides were chosen as the precursors of transition metals. Simultaneously, the metal chlorides served as acid modifiers and no mineral acids were added in the ethanol solution. Different kinds of transition metals were successfully introduced into the skeleton of mesostructure. The mesostructure and textural properties were detailed investigated by N_2-physisorption and TEM characterizations. The UV-vis diffuse reflectance spectra were employed for characterizing the oxidation states and coordination of transition metals in M-X-ZrPO. The obtained materials were employed as catalyst in the liquid phase oxidation of ethylbenzene. The heterogeneity and reusability of catalyst were also investigated. More details about the characterizations of these mesoporous materials and their catalytic properties are described specifically in the following text.

2. Experimental Section

2.1 Synthesis of M-X-ZrPO.

M-X-ZrPO was synthesized via an one-pot EISA method with F127 employed as structure-directing agents (SDAs).[24] In a typical procedure, 1.2 g of F127, 4.5 mmol of $ZrOCl_2 \cdot 8H_2O$, 0.5 mmol of metal chlorides ($CrCl_3 \cdot 6H_2O$, $MnCl_2 \cdot 4H_2O$, $FeCl_3 \cdot 6H_2O$, $CoCl_2 \cdot 6H_2O$, $NiCl_2 \cdot 6H_2O$, $CuCl_2 \cdot 2H_2O$ and $ZnCl_2$) and 3.75 mmol of $PO(OCH_3)_3$ were dissolved in 15 mL of anhydrous ethanol and vigorous stirred for 6 h without adding any mineral acids. Then the solution mixture was transferred to a drying oven to undergo the EISA process at 60 °C for 48 h and 100 °C for 24 h. The as-synthesized xerogel was calcined at 500 °C for 6 h with a heating rate of 1 °C·min^{-1} in air to remove SDAs. The obtained ordered mesoporous transition metals-zirconium oxophosphate composites were denoted as M-X-ZrPO (X = Cr, Mn, Fe, Co, Ni, Cu, Zn) and the nominal molar ratio of X% was 10% (molar ratio of X% = X_{mol} / (X_{mol} + Zr_{mol}) × 100%). In order to investigate the role of ordered mesostructure in promoting catalytic performance, the Mn-ZrPO material without adding F127 was synthesized as the aforementioned method and denoted as Mn-ZrPO-noF127.

2.2 Characterization.

The nitrogen adsorption and desorption isotherms were recorded on an Autosorb-iQ analyzer (Quantachrome Instruments U.S.). The specific surface area was calculated via Brunauer-Emmett-Teller (BET) method in the relative pressure range of 0.05-0.3; pore volume was calculated from adsorption isotherm at a relative pressure of 0.990; pore size distribution was calculated by Barrett-Joyner-Halenda (BJH) method.

Powder X-ray diffraction (XRD) measurements were performed on an X'Pert Pro

Multipurpose diffractometer (PANalytical, Inc.) with Cu Kα radiation (0.15406 nm) at room temperature from and 10.0° to 80.0°.

Transmission electron microscopy (TEM) images, selected area electron diffraction (SAED) and energy-dispersive X-ray spectroscopy (EDX) measurements were performed on the TECNAI G^2 F20 high-resolution transmission electron microscopy under a working voltage of 200 kV.

The element compositions were analyzed by X-Ray Fluorescence (XRF) spectrometer on a Magix PW2403 (PANalytical, Inc.).

UV-visible (UV-vis) diffuse reflectance spectra were recorded on a PE Lambda 650S instrument coupled with a diffuse reflectance accessory in the range of 190-850 nm.

2.3 Catalytic activity

The liquid phase oxidation of ethylbenzene was carried out in a round bottom flask fitted with water condenser. Initially, M-X-ZrPO (300 mg), acetonitrile (15 mL), ethylbenzene (9 mmol) and tert-Butyl hydroperoxide (36 mmol) were added to a 50 mL round bottom flask (the mass ratio of ethylbenzene to catalyst was 3.2). Then the reaction mixture was stirred at 80 ^{o}C for 24 h and the products were centrifuged and extracted with ether. The conversion of ethylbenzene and selectivity of products were monitored by a gas chromatography (GC) instrument (Agilent-7890A; equipped with a flame ionization detector (FID) and HP-5 column (30 m × 0.32 mm × 0.25 μm)) using octane as external. Gas chromatography-mass spectroscopy (GC-MS) instrument (5975c vl MSD with triple-axis detector, GC Agilent-7890A) was

employed to identify the reaction products. The separated catalyst was washed with ether and activated at 400 ^{o}C for 3 h for regeneration.

3. Results and discussion

Ordered M-X-ZrPO materials were synthesized via the facile EISA method employing F127 as SDAs (shown in Scheme 1). The $ZrOCl_2 \cdot 8H_2O$, metal chlorides and $PO(OCH_3)_3$ were chosen as precursors of metals and phosphorus. All the precursors and F127 were dissolved in the ethanol solvent and the transparent solution was gotten. Then the solution was transferred to an oven to undergo the EISA process. In this process, the solution turned into xerogel and the hydrophobic segments of F127 formed the cylindrical cores and all the precursors uniformly dispersed around the cores.[25] The F127 played a crucial role in the formation of mesoporous pores. The gotten xerogel was calcined under air atmosphere to remove the F127. At last, the M-X-ZrPO materials were obtained.

The ordered mesostructure of obtained M-X-ZrPO materials was characterized by N_2-physisorption technique. The N_2 adsorption-desorption isotherms and corresponding pore size distributions of M-X-ZrPO materials are presented in Fig.1. All the M-X-ZrPO samples exhibited typical IV isotherms and well-defined H1 hysteresis loops (IUPAC) with sharp capillary condensation steps at the relative pressure (p/p_o) of 0.4-0.8, indicating the existence of cylindrical mesoporous pores, which would be confirmed by the TEM images. The pore sizes of these samples were narrowly distributed at around 4-10 nm, implying the existence of uniform

mesoporous system. Moreover, the textural parameters, such as specific surface area, pore size and volume of M-X-ZrPO gotten from the N_2 adsorption-desorption isotherms are shown in Table 1. All the materials had excellent textural properties with large specific surface area (170-220 $m^2 \cdot g^{-1}$), big pore volume (0.2-0.4 $cm^3 \cdot g^{-1}$) and uniform pore size (5.6-7.8 nm). It was noteworthy that the introduced transition metals did not destroy the mesostructure. On the contrary, compared with M-ZrPO, the mesostructure of M-X-ZrPO was improved with the introduction of transition metals. Moreover, the Mn-ZrPO-noF127 was synthesized and employed as a comparison. Compared with M-Mn-ZrPO, the Mn-ZrPO-noF127 material showed poor textural properties (specific surface area (41.9 $m^2 \cdot g^{-1}$), pore size (2.52 nm) and volume (0.07 $cm^3 \cdot g^{-1}$)). Hence, the F127 played an essential role in constructing ordered mesoporous framework.

The XRD measurement of M-X-ZrPO was conducted to investigate the states of introduced transition metals species. As shown in Fig. 2, it was interesting that they only exhibited two broad and weak diffraction peaks in all the parents. The absence of obvious diffraction peaks of transition metals indicated that the introduced metals species were highly dispersed in the mesoporous skeleton. This might be on account of that transition metals atoms in the materials were segregated by zirconium and phosphorus atoms owing to the peculiar traits of one-pot EISA method. We deduced that the highly dispersed transition metals might be the reason for successful preservation of ordered mesostructure. Meanwhile, this could offer abundant active sites for the reactants.

In order to further confirm the presence of ordered mesopores in M-X-ZrPO, TEM (Fig. 3) images of the samples were taken. For all the samples, highly ordered cylindrical pores view along [110] and [001] orientations were observed, revealing a high degree of periodicity in large domains. These results of TEM observation agreed quite well with the N_2-physisorption characterization, which predicted the existence of cylindrical pores in these materials. Moreover, no obvious particles or aggregations of transition metals species were observed outside or inside of the channels for all the samples, illustrating the high dispersion of transition metals species in the materials. Therefore, it was concluded that metal species were highly dispersed in the mesoporous pore walls. This phenomenon further explained the absence of obvious diffraction peaks in XRD patterns of M-X-ZrPO. In addition, the EDX measurement and SAED pattern of M-Mn-ZrPO were studied as representatives. As shown in Fig. 3h, the characteristic peaks of Zr, P and Mn elements were obviously observed in the EDX profile of M-Mn-ZrPO, implying that all the elements were successfully introduced into the framework of mesostructure. In addition, all the transition metals molar ratios gotten from EDX measurement were shown in Table 1 and the values kept consistent with the ratios gotten from XRF characterizations and nominal values. This might be owing to that transition metals were homogeneously dispersed in the wall of mesostructure. For the corresponding SAED pattern of M-Mn-ZrPO (shown in Fig. 3i), there were no apparent electron diffraction rings, implying that the wall of mesoporous framework was amorphous, and further demonstrating the conclusion gotten from XRD.

The UV-vis diffuse reflectance spectra (shown in Fig. 4) were employed for characterizing the oxidation states and coordination of transition metals in M-X-ZrPO. As our previous report about M-ZrPO, the obvious adsorption band at 205 nm was designated to the Zr-O-P coordination and the weak band at about 300 nm could be attributed to Zr^{4+} interacting with the phosphate counter anions in the framework.[24] As the introduction of transition metals, additional bands appeared in the UV-vis spectra. For the M-Cr-ZrPO material, the bands at 270 and 370 nm were contributed to the ligand-metal charge transfer (LMCT) $O^{2-}\rightarrow Cr^{6+}$. The bands at 470 and 640 nm were owing to the $A_{2g}\rightarrow T_{1g}$ and $A_{2g}\rightarrow T_{2g}$ transitions of Cr^{3+} in octahedral symmetry, respectively.[26,27] For the spectra of M-Mn-ZrPO, the band at 270 nm showed the charge transfer transition of $O^{2-}\rightarrow Mn^{3+}$ with tetrahedral coordination. The broad band at about 500 nm was assigned to the d-d transition of Mn^{2+} in crystal field transition ($^6A_{1g}\rightarrow{}^4T_{2g}$).[21,28] The M-Fe-ZrPO showed an obvious band at 300 nm, which was owing to the LMCT that involved the isolated Fe^{3+} ions in tetrahedral coordination. The band at 470 nm was attributed to the oxygen to metal charge transfer (Fe^{3+}).[29] In the spectra of M-Co-ZrPO, the bands at 520, 580 and 640 nm were designated to the $^4A_2(F)\rightarrow{}^4T_1(P)$ transition characteristic of Co^{2+} ions in the isolated state with tetrahedral coordination.[22,30] The bands at 420 and 550 nm in the spectra of M-Ni-ZrPO were assigned to the two spin-allowed $^3A_{2g}\rightarrow{}^3T_{1g}(P)$ and $^3A_{2g}\rightarrow{}^3T_{1g}(F)$ of octahedrally coordinated Ni^{2+} ions (d^8).[31] For the M-Cu-ZrPO, the bands at 260 nm was assignable to the LMCT transitions between surface oxygen and isolated Cu^{2+} ions and the broad band at 600-850 nm was owing to d-d transitions of Cu^{2+} in a

tetragonally distorted octahedral environment.[32] No obvious absorption bands were observed in the spectra of M-Zn-ZrPO due to completely filled d^{10} electronic configuration of Zn^{2+} metal.[33]

The catalytic performance of M-X-ZrPO was investigated in liquid phase oxidation of ethylbenzene (EB) (shown in Scheme 2). In this reaction, the acetophenone (AP) was detected as the main product and a possible reaction mechanism was presented in Scheme 3.[34] The results of catalytic performance were shown in Fig. 5(1). The M-ZrPO showed poor catalytic performance, and only showed 9.7% conversion of EB and 16.9% selectivity of AP. With the introduction of transition metals, the catalytic performance was successfully improved, especially for the M-Cr-ZrPO and M-Mn-ZrPO, which showed the best activity (~90.0% conversion of EB and ~90.0% selectivity of AP). The sequence of catalytic activity was Cr, Mn, Cu, Co, Fe, Ni, Zn and this might be due to the different redox properties of transition metals. Moreover, it was noteworthy that the Mn-ZrPO-noF127, which had poor mesostructure, only showed 37.2% conversion of EB and 24.3% selectivity of AP. This indicated that the excellent mesoporous structure was in favor of improving the catalytic performance of M-X-ZrPO.

On account of the excellent catalytic performance of M-Mn-ZrPO, it was further employed for investigating the heterogeneity and reusability of catalyst. As shown in Fig. 5(2), the conversion of EB and selectivity of AP were gradually increased with time and reached the maximum at 24 h with the existing of catalyst. However, after filtering the catalyst from the reaction system at 3 h, there was no obvious increase in

conversion of EB and selectivity of AP even when the time reached up to 30 h. Meanwhile, as shown in Table 1, compared with the fresh catalyst, the Mn contents showed little change in the used catalyst (M-Mn-ZrPO-used). All these indicated that the M-Mn-ZrPO was truly a heterogeneous catalyst and no obvious Mn species leached into liquid phase in the reaction process.

The M-Mn-ZrPO was recycled for five runs and the results were shown in Fig. 5(3). There was no significant decrease in catalytic performance, showing the M-Mn-ZrPO could be reused as heterogeneous catalyst in the liquid phase oxidation of EB. In addition, the regenerated catalyst was characterized by N_2-physisorption and TEM (shown in Fig. 6). The results manifested that the ordered mesoporous structure with excellent textural properties and amorphous pore wall structure was successfully maintained. The catalyst showed excellent stability and the mesostructure suffered little influence in the reaction process. The high catalytic activity and stability of M-Mn-ZrPO might be owing to that the transition metals introduced from the EISA method were highly dispersed and firmly confirmed in the skeleton of mesoporous materials. The sintering and leaching of metal species in the calcination and reaction process could be largely avoided.

4. Conclusion

In this paper, a facile and general one-pot EISA method, which was suitable for different kinds of transition metals, was employed to synthesize a series of ordered M-X-ZrPO composites. All the transition metals species were homogeneously

dispersed in the skeleton of mesostructure and the ordered mesostructure with excellent textural properties were successfully maintained. The obtained ordered mesoporous materials exhibited excellent catalytic activity and reusability in the liquid phase oxidation of ethylbenzene. Therefore, the M-X-ZrPO might be excellent candidates of catalyst for selective oxidation reaction such as oxidation of ethylbenzene.

Acknowledgements

The authors sincerely acknowledge the financial supported by the "Strategic Priority Research Program" of the Chinese Academy of Sciences, Grant No. XDA09030101 and the National Natural Science Foundation of China (No. 21133011, 201373244).

Notes and references

[a] State Key Laboratory for Oxo Synthesis and Selective Oxidation, Lanzhou Institute of Chemical Physics, Chinese Academy of Sciences, Lanzhou 730000, People's Republic of China.

[b] University of Chinese Academy of Sciences, Beijing 100049, People's Republic of China.

[c] Suzhou Institute of Nano-Tech and Nano-Bionics, Chinese Academy of Sciences, Suzhou 215123, People's Republic of China.

[*]Corresponding author: e-mail: **ljchou@licp.cas.cn** (L. J. Chou), Tel: +86 0931 4968066; Fax: +86 0931 4968129

1. C. T. Kresge, M. E. Leonowicz, W. J. Roth, J. C. Vartuli and J. S. Beck, *Nature*, 1992, 359, 710-712.

2. J. S. Beck, J. C. Vartuli, W. J. Roth, M. E. Leonowicz, C. T. Kresge, K. D. Schmitt, C. T. W. Chu, D. H. Olson and E. W. Sheppard, *J. Am. Chem. Soc.*, 1992, 114, 10834-10843.

3. D. E. De Vos, M. Dams, B. F. Sels and P. A. Jacobs, *Chem. Rev.*, 2002, 102, 3615-3640.

4. M. E. Davis, *Nature*, 2002, 417, 813-821.

5. G. Wang, A. N. Otuonye, E. A. Blair, K. Denton, Z. Tao and T. Asefa, *J. Solid State Chem.*, 2009, 182, 1649-1660.

6. D. D. Asouhidou, K. S. Triantafyllidis, N. K. Lazaridis, K. A. Matis, S. S. Kim and T. J. Pinnavaia, *Micropor. Mesopor. Mater.*, 2009, 117, 257-267.

7. Y. Shi, Y. Wan and D. Zhao, *Chem. Soc. Rev.*, 2011, 40, 3854-3878.

8. D. Gu and F. Schuth, *Chem. Soc. Rev.*, 2014, 43, 313-344.

9. W. Cai, J. Yu, C. Anand, A. Vinu and M. Jaroniec, *Chem. Mater.*, 2011, 23, 1147-1157.

10. L. Xu, H. Song and L. Chou, *Catal. Sci. Technol.*, 2011, 1, 1032-1042.

11. S. K. Das, M. K. Bhunia, A. K. Sinha and A. Bhaumik, *ACS Catal.*, 2011, 1, 493-501.

12. A. Dutta, A. K. Patra, S. Dutta, B. Saha and A. Bhaumik, *J. Mater. Chem.*, 2012, 22, 14094-14100.

13. J. Wang, H. Li, H. Li, C. Zuo and H. Wang, *J. Phys. Chem. C*, 2012, 116, 9517-9525.

14. S. M. Grant and M. Jaroniec, *J. Mater. Chem.*, 2012, 22, 86-92.

15. B. Han, H. Wang, Y. Kong and J. Wang, *Mater. Lett.*, 2013, 100, 159-162.

16. J.-H. Shan, L. Chen, L. B. Sun and X. Q. Liu, *Energ. Fuel*, 2011, 25, 3093-3099.

17. E. Ramasamy and J. Lee, *Energy Environ. Sci.*, 2011, 4, 2529-2536.

18. J. H. Pan, X. Zhang, A. J. Du, H. Bai, J. Ng and D. Sun, *Phys. Chem. Chem. Phys.*, 2012, 14, 7481-7489.

19. S. Shen, J. Chen, R. T. Koodali, Y. Hu, Q. Xiao, J. Zhou, X. Wang and L. Guo, *Appl. Catal., B.*, 2014, 150-151, 138-146.

20. S. K. Mohapatra and P. Selvam, *J. Catal.*, 2007, 249, 394-396.

21. P. Visuvamithiran, K. Shanthi, M. Palanichamy and V. Murugesan, *Catal. Sci. Technol.*, 2013, 3, 2340-2348.

22. Y. Dong, X. Zhan, X. Niu, J. Li, F. Yuan, Y. Zhu and H. Fu, *Micropor. Mesopor. Mater.*, 2014, 185, 97-106.

23. M. P. Pachamuthu, V. V. Srinivasan, R. Maheswari, K. Shanthi and A. Ramanathan, *Catal. Sci. Technol.*, 2013, 3, 3335-3342.

24. Z. Miao, L. Xu, H. Song, H. Zhao and L. Chou, *Catal. Sci. Technol.*, 2013, 3, 1942-1954.

25. Z. X. Li, F. B. Shi, Y. Ding, T. Zhang and C. H. Yan, *Langmuir*, 2011, 27, 14589-14593.

26. D. Shee and A. Sayari, *Appl. Catal., A.*, 2010, 389, 155-164.

27. J. Baek, H. J. Yun, D. Yun, Y. Choi and J. Yi, *ACS Catal.*, 2012, 2, 1893-1903.

28. A. Kumar, D. Nepak and D. Srinivas, *Catal. Commun.*, 2013, 37, 36-40.

29. N. S. Sanjini and S. Velmathi, *RSC Adv.*, 2014, 4, 15381-15388.

30. H. Cui, Y. Zhang, Z. Qiu, L. Zhao and Y. Zhu, *Appl. Catal., B.*, 2010, 101, 45-53.

31. T. E. Klimova, D. Valencia, J. A. Mendoza-Nieto and P. Hernández-Hipólito, *J. Catal.*, 2013, 304, 29-46.

32. C. S. Chen, Y. T. Lai, T. W. Lai, J. H. Wu, C. H. Chen, J. F. Lee and H. M. Kao, *ACS Catal.*, 2013, 3, 667-677.

33. P. C. Sahoo, Y. N. Jang, Y. J. Suh and S. W. Lee, *J. Mol. Catal. A: Chem.*, 2014, 390, 105-113.

34. A. V. Biradar and T. Asefa, *Appl. Catal., A.,* 2012, 435-436, 19-26.

Table 1. Textural properties of M-X-ZrPO derived from nitrogen physisorption and molar ratios of transition metals gotten from XRF and EDX.

Sample	Specific surface area ($m^2 \cdot g^{-1}$)	Pore size (nm)	Pore volume ($cm^3 \cdot g^{-1}$)	Nominal molar ratios	Ratios from XRF	Ratios from EDX
M-ZrPO	160.0	5.64	0.26	—	—	—
M-Cr-ZrPO	216.6	6.55	0.28	0.100	0.095	0.092
M-Mn-ZrPO	189.1	6.54	0.28	0.100	0.102	0.090
M-Fe-ZrPO	192.7	5.65	0.22	0.100	0.103	0.103
M-Co-ZrPO	200.6	6.56	0.29	0.100	0.102	0.107
M-Ni-ZrPO	193.4	6.55	0.30	0.100	0.103	0.089
M-Cu-ZrPO	206.3	7.77	0.37	0.100	0.098	0.095
M-Zn-ZrPO	177.0	6.56	0.29	0.100	0.097	0.094
M-Mn-ZrPO-used	164.5	6.56	0.27	0.100	0.099	0.091
Mn-ZrPO-noF127	41.9	2.52	0.07	0.100	0.106	0.135

Figure captions:

Figure 1. (1) N_2 physisorption isotherms and **(2)** pore size distributions of M-X-ZrPO: **(a)** M-ZrPO, **(b)** M-Cr-ZrPO, **(c)** M-Mn-ZrPO, **(d)** M-Fe-ZrPO, **(e)** M-Co-ZrPO, **(f)** M-Ni-ZrPO, **(g)** M-Cu-ZrPO and **(h)** M-Zn-ZrPO.

Figure 2. XRD patterns of M-X-ZrPO: **(a)** M-ZrPO, **(b)** M-Cr-ZrPO, **(c)** M-Mn-ZrPO, **(d)** M-Fe-ZrPO, **(e)** M-Co-ZrPO, **(f)** M-Ni-ZrPO, **(g)** M-Cu-ZrPO and **(h)** M-Zn-ZrPO.

Figure 3. TEM images of M-X-ZrPO: **(a)** M-Cr-ZrPO, **(b)** M-Mn-ZrPO, **(c)** M-Fe-ZrPO, **(d)** M-Co-ZrPO, **(e)** M-Ni-ZrPO, **(f)** M-Cu-ZrPO and **(g)** M-Zn-ZrPO; EDX measurement **(h)** and SAED pattern **(i)** of M-Mn-ZrPO.

Figure 4. UV-vis diffuse reflectance spectra of M-X-ZrPO: **(a)** M-ZrPO, **(b)** M-Cr-ZrPO, **(c)** M-Mn-ZrPO, **(d)** M-Fe-ZrPO, **(e)** M-Co-ZrPO, **(f)** M-Ni-ZrPO, **(g)** M-Cu-ZrPO and **(h)** M-Zn-ZrPO.

Figure 5. Liquid phase oxidation of ethylbenzene: **(1)** catalyzed by M-X-ZrPO and Mn-ZrPO-noF127; **(2)** catalyzed by M-Mn-ZrPO at different time; **(3)** the recyclability of M-Mn-ZrPO.

Figure 6. (1) isotherms; **(2)** pore size distribution; **(3)** and **(4)** TEM images and SAED pattern of M-Mn-ZrPO-used.

Scheme 1. Schematic illustration for the M-X-ZrPO synthesized from EISA method.

Scheme 2. Liquid phase oxidation of ethylbenzene over M-X-ZrPO catalyst.

Scheme 3. A possible reaction mechanism of liquid phase oxidation of ethylbenzene over M-Mn-ZrPO catalyst.

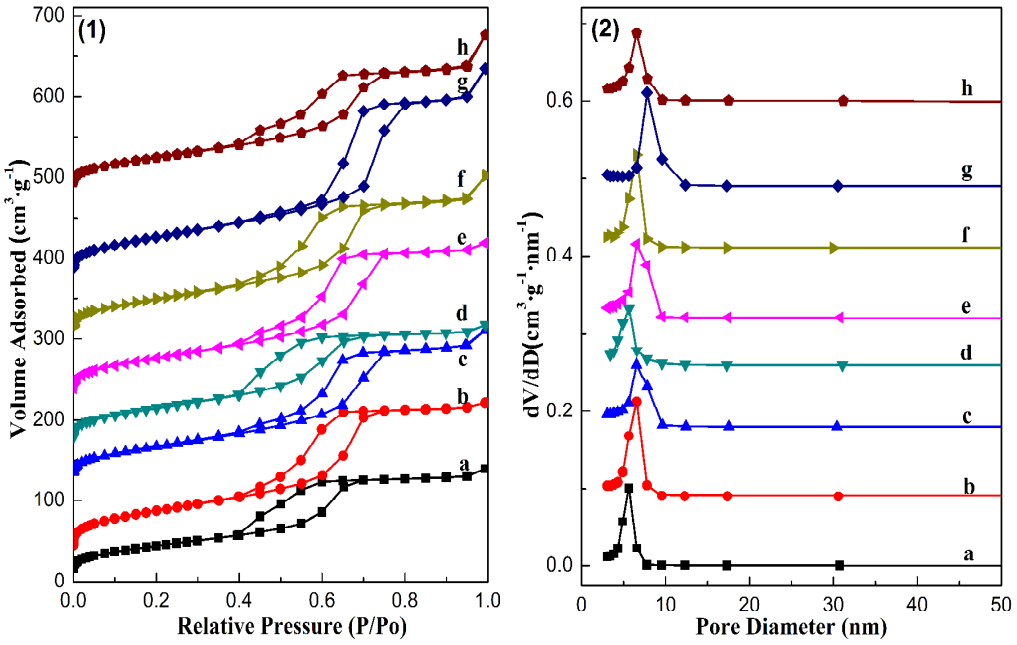

Figure 1

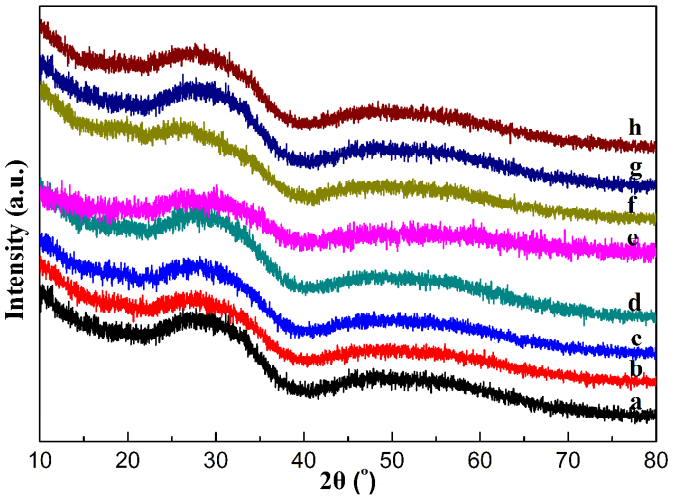

Figure 2

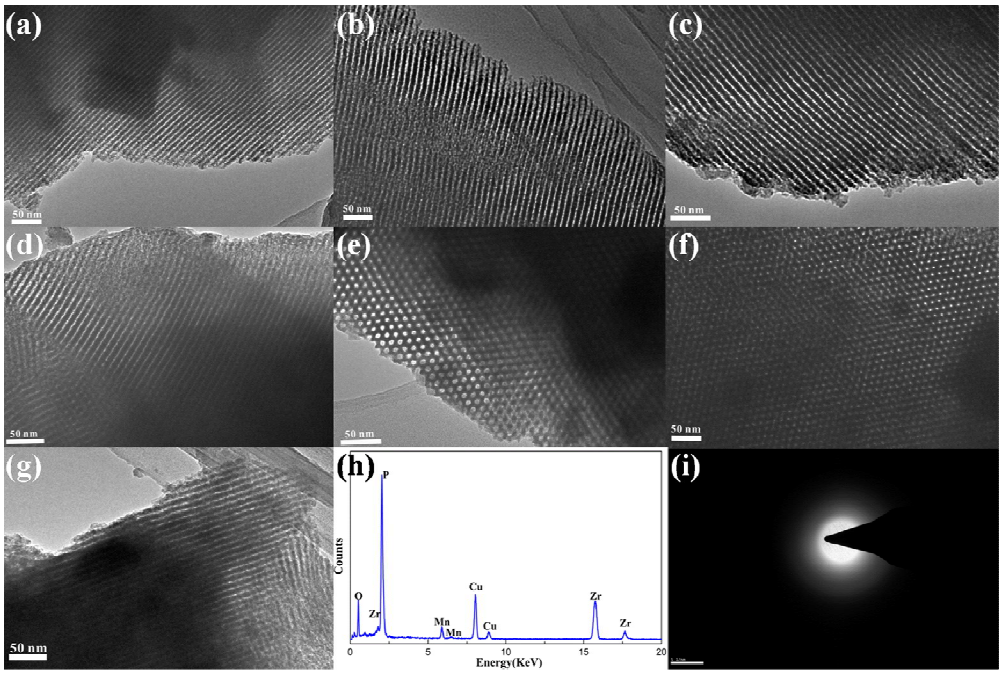

Figure 3

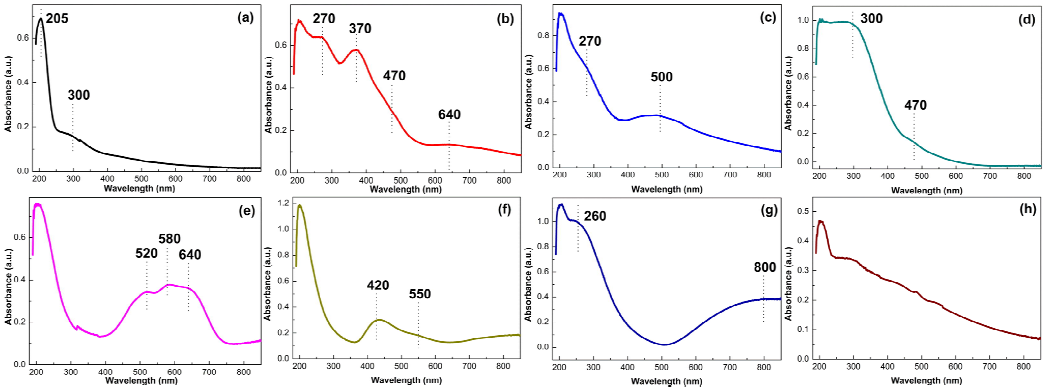

Figure 4

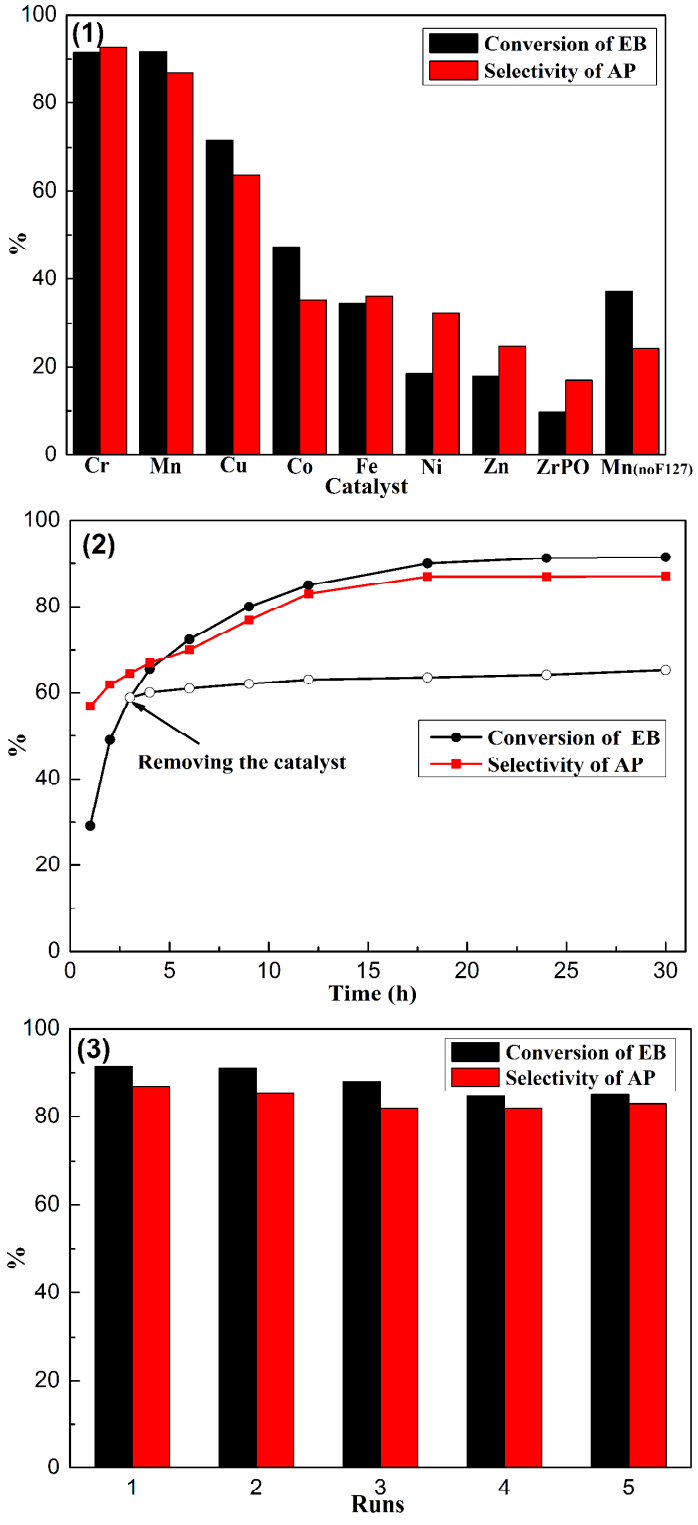

Figure 5

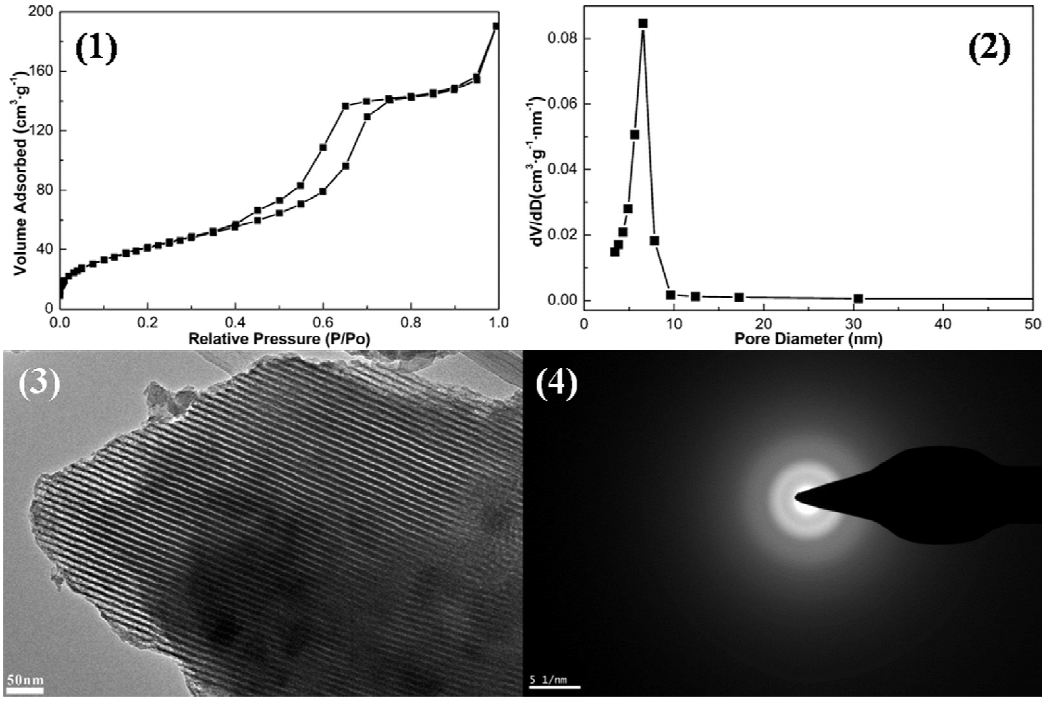

Figure 6

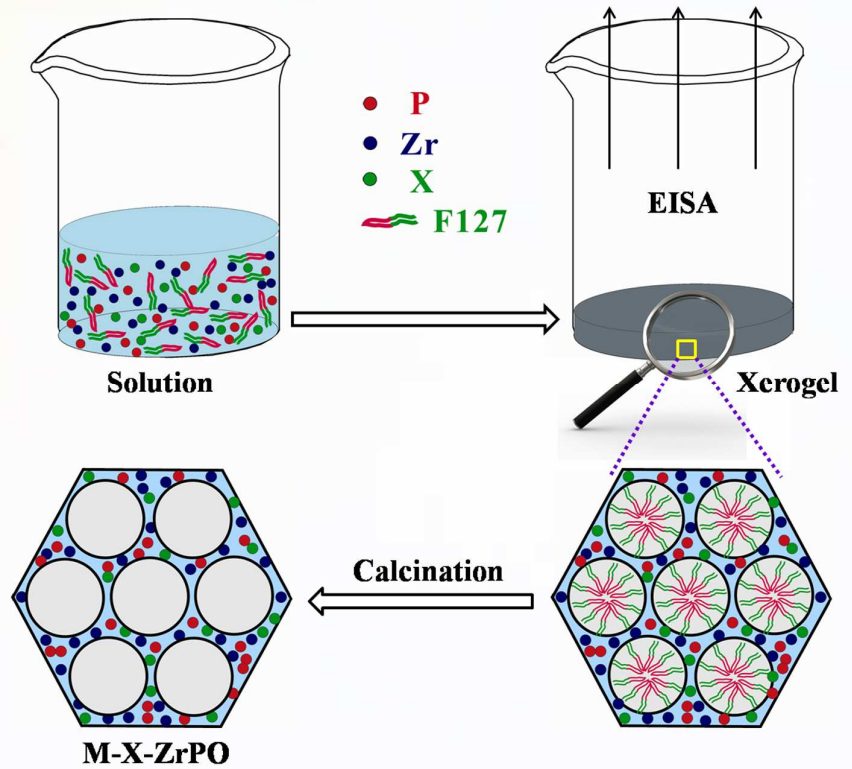

Scheme 1

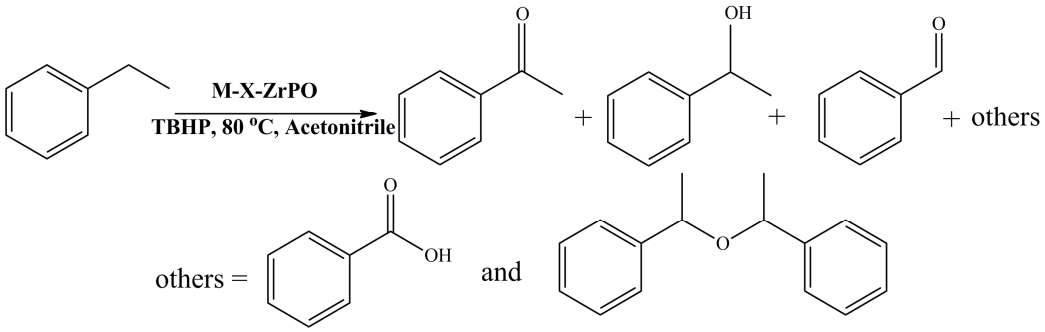

Scheme 2

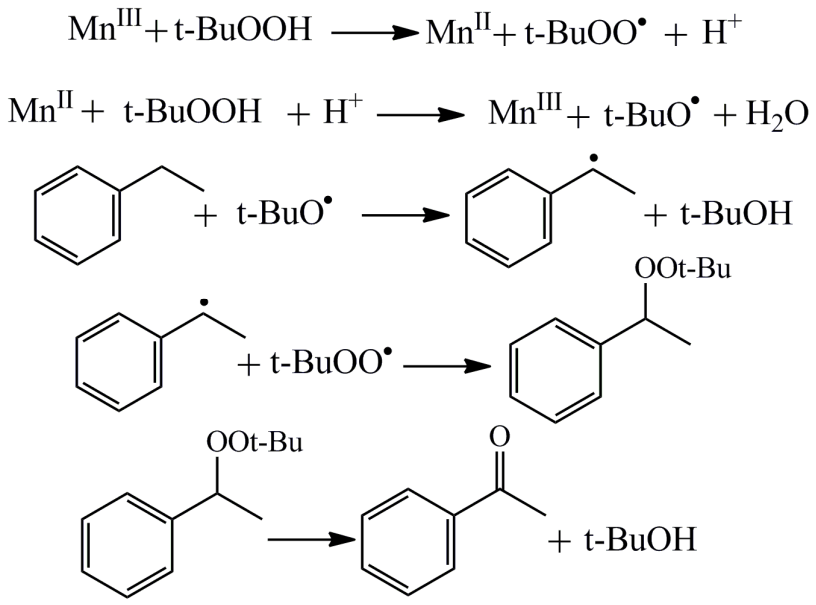

Scheme 3

The image for TOC

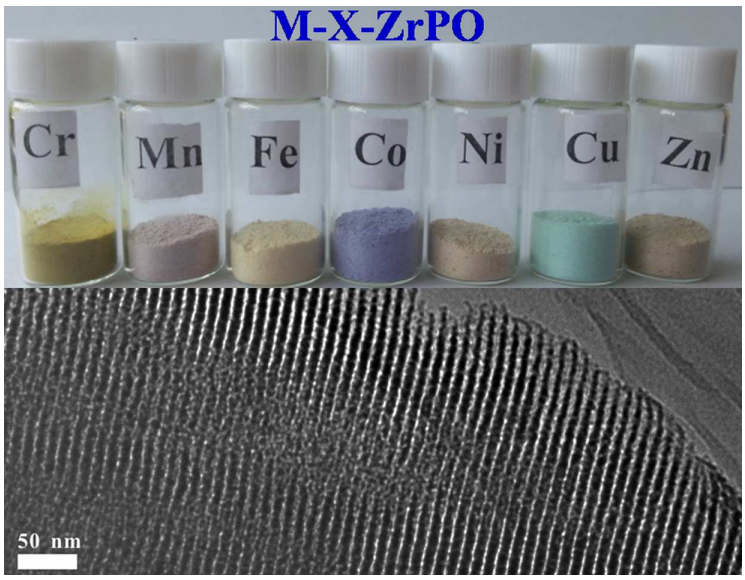

A series of ordered M-X-ZrPO materials were successfully synthesized via a facile and general one-pot evaporation-induced self-assembly (EISA) strategy.